Suboptical Wavelength Position Measurement of Moving Atoms Using Optical Fields

J. R. Gardner, M. L. Marable, G. R. Welch,[a] and J. E. Thomas
Physics Department, Duke University, Durham, North Carolina 27708-0305
(Received 16 February 1993)

We demonstrate all-optical techniques for position measurement and localization of moving atoms with suboptical wavelength precision. Spatial resolution of 200 nanometers, with linearity over a few microns, is obtained by the methods which ultimately will scale to yield nanometer resolution limited by the uncertainty principle.

PACS numbers: 42.50.Vk, 32.80.Pj

In this Letter, we demonstrate new optical techniques for precision position measurement and state selective localization of moving atoms. The methods employ Raman-induced resonance imaging [1–3] in which a spatially varying potential correlates an atomic resonance frequency with the atomic position. Optical methods are ideally suited for high-resolution resonance imaging because they permit the study of very small volumes, which facilitates the use of spatially varying potentials with very large gradients. Further, these optical techniques eliminate the need to place mechanical surfaces (slits, wires, etc.) in the region to be studied. The current experiments demonstrate a new method of imaging which employs a spatially varying light shift to achieve spatial resolution of 200 nanometers, with linearity over a few microns. Centroids of localized atomic distributions, which are created and measured in the experiments, are determined (from the χ^2 fits) with an accuracy of ± 20 nanometers. This breakthrough paves the way for new experiments employing still larger gradients and single atom detection, which are expected to achieve nanometer spatial resolution, limited by the uncertainty principle [2].

The motivation for developing these techniques lies in the recent progress and interest in the de Broglie wave optics of neutral atoms, which is rapidly emerging as one of the most exciting new fields in atomic and optical physics [4]. There has been a great deal of work done in such areas as atomic diffraction [5], spectroscopy in standing waves [6], spatial rephasing [7], channeling [8], focusing [9], and interferometry [10]. In addition, the great strides made in laser cooling [11] have recently made possible the study of quantized atomic states in traps [12–14], while recent progress in neutral atom lithography [15] suggests applications such as controlled microfabrication of structures using neutral atomic beams. All of these techniques are capable of producing atomic spatial patterns that vary over very small length scales. Prior to the resonance imaging technique presented here and in Refs. [1–3], there have been no general experimental methods for position measurement in atomic beams or traps which achieve the spatial resolution required for direct measurement of the atomic spatial distributions. Recently, an alternative scheme has been suggested, theoretically, that determines atomic positions by measuring the phase shift of the optical field in a cavity due to a position dependent atom-field coupling [16].

The basic imaging technique which we are developing, Figs. 1 and 2, employs a light-shift gradient region comprised of a single $\hat{\mathbf{z}}$ polarized laser beam, focused with a cylindrical lens. The current experiments were carried out in atomic samarium (^{152}Sm), for which the nuclear spin is zero, using the $^7F_1 \rightarrow {}^7F_0$ transition at 570.68 nm (Fig. 1). Raman transitions are induced between a long lived initial state i ($M_J = -1$) and a long lived final state f ($M_J = 0$). The final state f is initially emptied by optical pumping and is shifted in proportion to the light-shift beam intensity, which varies rapidly along the $\hat{\mathbf{x}}$ axis perpendicular to the atomic beam. Raman transitions occur in a localized region of width Δx along the measurement $\hat{\mathbf{x}}$ axis, near the point where the light-shifting field tunes the level splitting between the initial and final states into resonance with the applied Raman field difference frequency. Atoms entering the Raman region in the initial state i are unaffected by the light-shifting field, thereby avoiding unwanted scattering of the incident atomic distribution. Atoms which make a Raman transition into

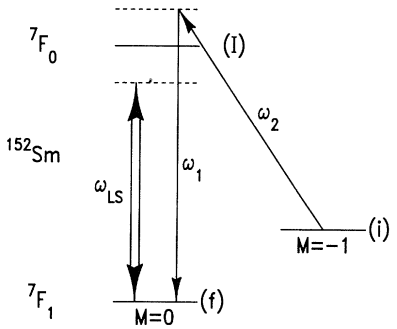

FIG. 1. Energy levels of ^{152}Sm used for Raman induced resonance imaging. A uniform magnetic field splits the $M_J = -1$ level, i, and the $M_J = 0$ level, f, by $\simeq 220$ MHz. An off-resonant light field ω_{LS} shifts the energy of the final ($M_J = 0$) state, f.

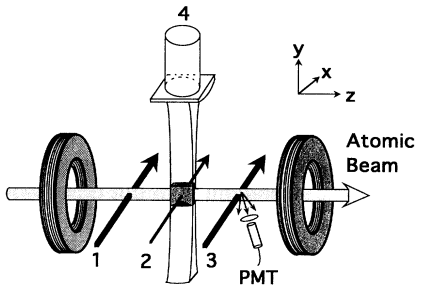

FIG. 2. Experimental arrangement. An intense, off-resonant light field (4) is focused with a cylindrical lens to yield a spatial variation of the energy of state f, with a constant gradient over a few microns. Raman fields (2) induce transitions between levels i and f in a localized region along the $\hat{\mathbf{x}}$ axis. The number of atoms emerging in state f, which is initially emptied by optical pumping (1), is measured by resonance fluorescence (3) as a function of Raman difference frequency to determine the spatial distribution in state i.

the final state f are detected downstream by resonance fluorescence and photon counting. By measuring the resonance fluoresence intensity as a function of the Raman fields difference frequency, $\omega_1 - \omega_2$, the spatial distribution of atoms in the initial state is determined.

Generally, the number N_f of atoms emerging in the final state can be written in the simple form

$$N_f = \eta_R \int\int dx\, dv_x\, R(x - x_0, v_x)\, \rho_i(x, v_x), \qquad (1)$$

where η_R is the Raman transition probability in the absence of the light-shift gradient. Equation (1) shows that the number of final state atoms is proportional to the convolution of a resolution function R, which is sharply peaked at a selected point x_0, with the initial state Wigner phase space distribution $\rho_i(x, v_x)$, specified at the center of the Raman region. The point x_0 is the point in space where the Raman transition is resonant with the applied optical fields. As shown below, the spatial resolution and hence the width of the resolution function must be dependent on the initial velocity along the measurement axis. Hence, the initial state phase space distribution must be specified in the measurement region. The resolution function is given generally by Eq. (19) of Ref. [2] which includes the effects of atomic velocity, acceleration, and diffraction.

As discussed previously [1–3], the ultimate spatial resolution of this method (i.e., the width of the spatial resolution function) can be estimated by heuristic arguments. Assuming that the light shift varies linearly over a limited region, the energy of the final state can be written as $V_f(x) = V_0 - (x - x_0)F$, where F is the force exerted on the final state. For a position change Δx, the Raman resonance frequency changes by $F\Delta x/\hbar$. The position change will be just resolvable when this frequency change is equal to the spectral resolution $\Delta\omega$. For long lived initial and final states, $\Delta\omega = 1/T$, where T is the transit time across the Raman region. Hence, the position resolution is $\Delta x = \hbar/(FT)$. To achieve resolution Δx for an atom with constant x velocity, v_x, the maximum transit time must be limited to $T = \Delta x/v_x$, which implies that the optimum resolution is of order $\sqrt{\hbar v_x/F}$. A more careful calculation [2] for Gaussian Raman beams with an intensity $1/e$ radius d yields the spatial resolution function for this case in the form

$$R(x - x_0, v_x) = \frac{1}{\sqrt{1 + \left(\frac{d}{d_{\rm opt}}\right)^4}} \exp\left[-\frac{(x - x_0)^2}{\Delta x^2}\right] \qquad (2)$$

with

$$\Delta x = \Delta x_{\rm VEL} \sqrt{\frac{1}{2}\left(\frac{d}{d_{\rm opt}}\right)^2 + \frac{1}{2}\left(\frac{d_{\rm opt}}{d}\right)^2}, \qquad (3)$$

where the optimum velocity limited resolution is given by $\Delta x_{\rm VEL} = \sqrt{2\hbar v_x/F}$, the optimum $1/e$ intensity radius of the Raman beams is $d_{\rm opt} = \Delta x_{\rm VEL}/\theta$, and $\theta \equiv v_x/v_y$.

The experiments utilize a supersonic beam of samarium atoms (speed 9×10^4 cm/sec, spread 7%), collimated to 100 μrad divergence. Raman transitions are induced between the $J = 1, M_J = -1$ and $J = 1, M_J = 0$ states using copropagating $\hat{\mathbf{z}}$ and $\hat{\mathbf{y}}$ polarized optical fields, each of intensity $1/e$ radius d, differing in frequency by $\simeq 220$ MHz, and tuned 110 MHz above their respective resonance frequencies with the excited $^7F_0$ state. These beams are derived by acousto-optic modulation from a common laser source to eliminate jitter in the difference frequency [17]. Further, they are combined in a single-mode, polarization preserving fiber to ensure that they are copropagating and thus eliminate any Doppler broadening due to misalignment of the Raman beams with each other.

The light-shifting region consists of a 100 mW, 9.5 mm diameter (FWHM) $\hat{\mathbf{z}}$ polarized Gaussian laser beam, propagating in the $\hat{\mathbf{y}}$ direction and focused with a cylindrical lens to a diameter of $B = 15.8$ μm (FWHM) along the measurement $\hat{\mathbf{x}}$ axis. The diameter, B, is measured using a 1 μm diam pinhole translated across the focus by a differential micrometer calibrated in 0.5 μm intervals. The frequency is tuned 110 MHz below resonance from the $^7F_1, M_J = 0 \rightarrow {}^7F_0$ transition. The Raman difference frequencies are adjusted so that transitions occur near the maximum derivative points for the intensity of the Gaussian light-shifting beam, i.e., at $x = x_0 = \pm B/2\sqrt{2\ln 2}$. Near this point, the force F is locally constant and can be estimated from the shift in the $J = 1, M_J = 0$ state using $F = -(\partial/\partial x)(h\beta/2)$. Here $\beta = \sqrt{\Delta^2 + \Omega^2(x, z)}$ is the generalized Rabi frequency in Hz, $\Omega(x, z)$ is the spatially varying Rabi frequency, and F is evaluated at $x = x_0$ and $z = 0$. With the above parameters, and the 342 nsec spontaneous lifetime of the $^7F_0$ state, the light shift causes a frequency shift of the $^7F_1$, $M = 0$ state of

$F/h = 11.6$ GHz/cm $= 1.16$ MHz/μm which varies by less than 10% over a 3 μm interval centered about the maximum derivative point.

To demonstrate the spatial resolution of this method, two Raman regions are employed in the light-shift region. The first region burns two Gaussian spatial holes in the $M_J = -1$ state population near the maximum derivative points in the light-shifting beam intensity, and creates corresponding population peaks in the initially empty $M_J = 0$ state. The second Raman region measures the narrow spatial distributions created by the first. Since the preparation and measurement regions utilize the same light-shift field, mechanical vibration of the relative position is eliminated. When the second Raman field difference frequency is unequal to that of the first region, both Raman regions add population to the final $M_J = 0$ state, causing the signal in the $M_J = 0$ detection region to remain constant as the second Raman region frequency difference is scanned. However, when the second Raman field difference frequency approaches that of the first region, a resonant decrease in the $M_J = 0$ state signal occurs as the hole created in the first region is probed by the second. The fluoresence signal obtained as a function of the difference frequency of the second Raman region is plotted in Fig. 3, using the calculated light-shift gradient of 1.16 MHz/μm to convert the frequency scale to position units. The diameter of the Raman regions is $D = 2.5$ mm (FWHM) and the regions are overlapped to minimize broadening due to ballistic expansion. The half width at $1/e$ of the fitted Gaussian distribution (solid curve) is $\sqrt{2}\times$ 200 nm. Since the measured distribution according to Eq. (1) is the convolution of a Gaussian distribution created in the first Raman region with a Gaussian spatial resolution function of identical width for the second region, the $1/e$ width for the spatial distribution in either region must be 200 nm.

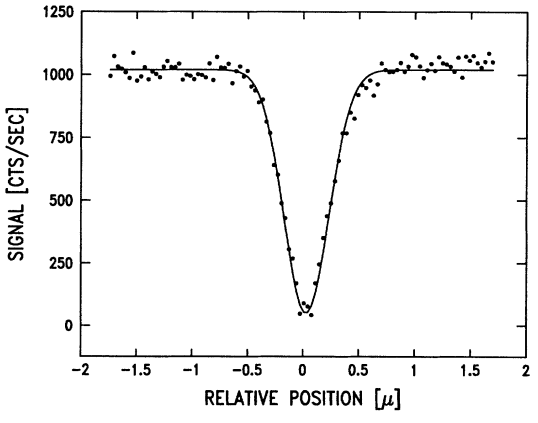

FIG. 3. Atomic localization by resonance imaging in a light-shift gradient. The horizontal scale is calibrated using the calculated light-shift gradient which is 1.16 MHz/μm. The dots are the experimental data. The solid curve is a fit using a Gaussian with a half-width at $1/e$ of $\sqrt{2}\,\Delta x$, where $\Delta x = 200$ nm.

To check the calibration of the position scale, additional experiments were conducted with the light-shifting region rotated by an angle θ with respect to the atomic beam axis using a differential micrometer to obtain angles of 0.1–1 mrad. Two Raman regions of $D = 1.3$ mm (FWHM) diameter, which optimizes the spatial resolution for an angle of 1 mrad ($v_x = 90$ cm/sec), were separated by a distance $S = 2$ mm between centers. In this case, the narrow spatial distributions created in the first Raman region move along the x axis a distance θS in propagating to the second Raman region. The narrow packet created on one side of the Gaussian light-shifting beam moves toward higher light shift, while the packet created on the other side moves toward lower light shift. This splits the spectrum obtained by scanning the frequency of the second Raman region as shown in Fig. 4. The splitting should correspond to a distance $2\theta S$, since the slopes on opposite sides of the Gaussian light-shifting beam are opposite in sign. Using an angle of 2/3 mrad, the expected splitting is 8/3 μm $= 2.7$ μm. This is in excellent agreement with the 2.5 μm obtained from the data using the calculated light-shift gradient in Fig. 4.

The measured spatial widths of the resolution functions for Figs. 3 and 4 can be compared with those calculated using Eq. (3) for the given Raman beam diameters and angles θ of the light-shifting region. At $\theta = 0$, the atomic beam divergence (0.1 mrad) leads to a velocity $v_x \simeq 10$ cm/sec. With $D = 2.5$ mm, Fig. 3, transit-time broadening and atomic motion contribute equally to the

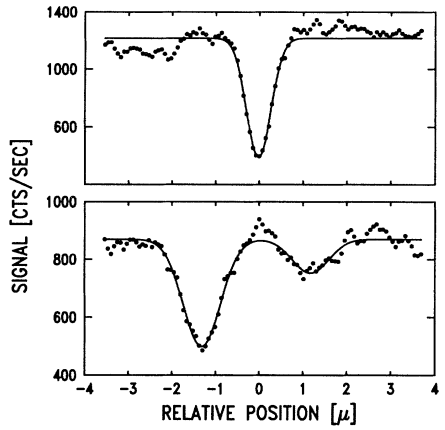

FIG. 4. Mechanical calibration of the light-shift gradient. Rotating the cylindrical lens by an angle θ causes one of the atomic packets created on the sides of the Gaussian light-shifting beam to move to higher light shift, while the other moves to lower light shift, causing the Raman spectrum to split. The distance between the peaks corresponds to twice the distance each packet moves, confirming the calculated light-shift gradient. The dots are the experimental data and the solid curves are fitted Gaussians with a half-width at $1/e$ of $\sqrt{2}\,\Delta x$, where Δx is given in Table I. Upper curve: $\theta = 0$; lower curve: $\theta = 2/3$ mrad.

TABLE I. Spatial resolution. Note that $D = 2\sqrt{\ln 2}\, d$.

θ (mrad)	D_{FWHM} (mm)	$\Delta x_{1/e}$ (calc.) (nm)	$\Delta x_{1/e}$ (meas.) (nm)
0.1 (divergence)	2.5	170	200
0.1 (divergence)	1.3	260	280
0.67	1.3	450	420

spatial resolution. With $D = 1.3$ mm, Fig. 4, the spatial resolution is dominated by transit time broadening. Thus, it is insensitive to the exact beam divergence and to ballistic expansion due to propagation between the Raman regions, as verified by a detailed calculation. For $\theta = 2/3$ mrad, $v_x \simeq 68$ cm/sec, and the resolution is dominated by the atomic beam speed along the measurement axis and transit-time broadening, again rendering ballistic expansion unimportant. Results calculated directly from Eq. (3) for the $1/e$ width of the resolution function using the calculated light-shift gradient of $F/h = 11.6$ GHz/cm, are given in Table I. These agree quite well with the $1/e$ widths of the Gaussian distributions which are fit to the data, after dividing by a factor $\sqrt{2}$ as described above. In Fig. 4 one notes that the right peak which occurs on the high light-shift part of the spectrum, is smaller than the left peak, which corresponds to low light shift. This feature can be explained qualitatively as due to optical pumping by the light-shifting field, which in not tuned sufficiently off resonance at the highest intensities in the present experiments.

In conclusion, we have demonstrated that Raman induced resonance imaging in a light-shift gradient is capable of extremely high spatial resolution and provides a general, state selective method for position measurement and localization of moving atoms. Single atom detection for the final state and still higher light-shift gradients will permit scaling to nanometer spatial resolution limited by atomic diffraction and acceleration [2]. Such resolution will find interesting applications in the imaging of atomic spatial distributions created in a variety of atom optics experiments, including the development of novel atom optical elements, two point correlation techniques, and imaging in traps. Techniques for spectroscopy of atoms in spatially varying fields also can be developed that use atomic localization to eliminate broadening due to spatial inhomogeneity. Minimum uncertainty packets, which can be created under certain conditions [2], may find important applications in creating controllable, focused atom beams. Combining state selective localization with state selective chemical reactions may permit high resolution position dependent chemistry. These methods also will find important practical applications in ultrahigh resolution neutral atom lithography.

This work is supported by ARO Grant No. DAAL03-90-G-0114, NIST Grant No. 60NANB0D1053, and RADC Contract No. F19628-88-K-0012.

[a] Permanent address: Department of Physics, Texas A&M University, College Station, TX 77843.

[1] J. E. Thomas, Opt. Lett. **14**, 1186 (1989).
[2] J. E. Thomas, Phys. Rev. A **42**, 5652 (1990).
[3] K. D. Stokes, C. Schnurr, J. R. Gardner, M. Marable, G. R. Welch, and J. E. Thomas, Phys. Rev. Lett. **67**, 1997 (1991).
[4] For a recent review, see the special issue on atom optics in Appl. Phys. B **54** (1992).
[5] P. E. Martin, B. G. Oldaker, A. H. Miklich, and D. E. Pritchard, Phys. Rev. Lett. **60**, 515 (1988).
[6] M. G. Prentiss and S. Ezekiel, Phys. Rev. Lett. **56**, 46 (1986).
[7] V. P. Chebotayev, B. Ya. Dubetsky, A. P. Kasantsev, and V. P. Yakovlev, J. Opt. Soc. Am. B **2**, 1791 (1985).
[8] C. Salomon, J. Dalibard, A. Aspect, H. Metcalf, and C. Cohen-Tannoudji, Phys. Rev. Lett. **59**, 1659 (1987).
[9] V. I. Balykin and V. S. Letokhov, Phys. Today **42**, No. 4, 23 (1989).
[10] O. Carnal and J. Mlynek, Phys. Rev. Lett. **66**, 2689 (1991); D. W. Keith, C. R. Ekstrom, Q. A. Turchette, and D. E. Pritchard, Phys. Rev. Lett. **66**, 2693 (1991); M. Kasevich and S. Chu, Phys. Rev. Lett. **67**, 181 (1991).
[11] See for example, W. D. Phillips, J. V. Prodan, and H. J. Metcalf, J. Opt. Soc. Am. B **2**, 1751 (1985).
[12] D. Grison, B. Lounis, C. Salomon, J.-Y. Courtois, and G. Grynberg, Europhys. Lett. **15**, 149 (1991).
[13] P. Verkerk, B. Lounis, C. Salomon, C. Cohen-Tannoudji, J.- Y. Courtois, and G. Grynberg, Phys. Rev. Lett. **68**, 3864 (1992).
[14] P. S. Jessen, C. Gerz, P. D. Lett, W. D. Phillips, S. L. Rolston, R. J. C. Spreeuw, and C. I. Westbrook, Phys. Rev. Lett. **69**, 49 (1992).
[15] G. Timp, R. E. Behringer, D. M. Tennant, J. E. Cunningham, M. Prentiss, and K. K. Berggren, Phys. Rev. Lett. **69**, 1636 (1992).
[16] P. Storey, M. Collett, and D. Walls, Phys. Rev. Lett. **68**, 472 (1992); M. A. M. Marte and P. Zoller, Appl. Phys. B **54**, 477 (1992).
[17] J. E. Thomas, P. R. Hemmer, S. Ezekiel, C. C. Leiby, Jr., R. H. Picard, and C. R. Willis, Phys. Rev. Lett. **48**, 867 (1982).